ChemPubSoc Europe

DOI: 10.1002/chem.201705921

CHEMISTRY A European Journal Full Paper

Density Functional Calculations

Identifying On-Surface Site-Selective Chemical Conversions by Theory-Aided NEXAFS Spectroscopy: The Case of Free-Base Corroles on Ag(111)

H. Aldahhak[+],*[a] M. Paszkiewicz[+],[b] E. Rauls,[c] F. Allegretti,[b] S. Tebi,[d] A. C. Papageorgiou,[b] Y.-Q. Zhang,[b] L. Zhang,[b] T. Lin,[b] T. Paintner,[b] R. Koch,[d] W. G. Schmidt,[a] J. V. Barth,[b] W. Schöfberger,[e] S. Müllegger,[d] F. Klappenberger,*[b] and U. Gerstmann[a]

Abstract: We demonstrate here that theory-assisted near-edge X-ray absorption fine-structure (NEXAFS) spectroscopy enables the site-sensitive monitoring of on-surface chemical reactions, thus, providing information not accessible by other techniques. As a prototype example, we have used free-base 5,10,15-tris(pentafluorophenyl)corroles (3H-TpFPC) adsorbed on Ag(111) and present a detailed investigation of the angle-dependent NEXAFS of this molecular species as well as of their thermally induced derivatives. For this, we have recorded experimental C and N K-edge NEXAFS spectra and interpret them based on XAS cross-section calculations by using a continuous fraction approach and core-hole including multiprojector PAW pseudopotentials within DFT. We have characterized the as-deposited low temperature (200 K) phase and unraveled the subsequent changes induced by dehydrogenation (at 330 K) and ring-closure reactions (at 430 K). By exemplarily obtaining profound insight into the on-surface chemistry of free-base corrolic species adsorbed on a noble metal this work highlights how angle-dependent XAS combined with accurate theoretical modeling can serve for the investigation of on-surface reactions, whereby even highly similar molecular structures, such as tautomers and isomers, can be distinguished.

Introduction

Corroles are tetrapyrrole macrocycles with a broad range of applications in various fields of science from physics and chemistry to bioscience and medicine.[1–7] After the first synthesis of corroles more than 50 years ago,[8] rich chemistry related to their peculiarity,[9–13] namely the stabilization of high-valent metal states promoting oxidation reactions,[14–16] has been investigated with steadily increasing effort.[14,17–22] There are also investigations that consider well-defined interfaces formed by corroles adsorbed on clean substrates under ultra-high vacuum (UHV) conditions.[23–29] In particular, the adsorption of the prototypical free-base corrole, namely the 5,10,15-tris(pentafluorophenyl)corrole (3H-TpFPC) (Figure 1), on Ag(111) has recently been investigated both in the multilayer[27] as well as in the (sub)monolayer regime.[28,29] In the latter case, many intriguing results regarding the nontrivial self-assembled molecular structures and on-surface chemical reactions have been observed. In the temperature range between 200 and 700 K at least four thermally induced structural transformations are observed, from hydrogen release originating at pyrrolic N–H bonds (≈300 K), over (multiple) ring-closure reactions between the fluorophenyl rings and the macrocycle (above 430 K), up to the formation of intermolecularly linked networks (above 550 K).

X-ray photoelectron spectroscopy (XPS) offers the sensitivity to address (sub)monolayer samples and thus was often employed to identify or corroborate on-surface reactions. However, for systems in which a reaction could occur at several equivalent places it is challenging to achieve site-selectivity, that is, to identify where a reaction has taken place.

Near-edge X-ray absorption fine-structure (NEXAFS) measurements can provide valuable complementary information on

[a] H. Aldahhak,[+] Prof. Dr. W. G. Schmidt, Dr. U. Gerstmann
Department of Physics, Paderborn University, Warburger Strasse 100, 33095 Paderborn (Germany)
E-mail: aldahhak@upb.de

[b] M. Paszkiewicz,[+] Dr. F. Allegretti, Dr. A. C. Papageorgiou, Dr. Y.-Q. Zhang, L. Zhang, Dr. T. Lin, T. Paintner, Prof. Dr. J. V. Barth, Dr. F. Klappenberger
Physics Department E20, Technical University of Munich
D-85748 Garching (Germany)
E-mail: florian.klappenberger@tum.de

[c] Prof. E. Rauls
Department of Mathematics and Natural Science
University of Stavanger, Stavanger (Norway)

[d] Dr. S. Tebi, Prof. Dr. R. Koch, Prof. S. Müllegger
Institute of Semiconductor and Solid State Physics
Johannes Kepler University Linz, Altenberger Strasse 69
4040 Linz (Austria)

[e] Prof. Dr. W. Schöfberger
Institute of Organic Chemistry, Johannes Kepler University Linz
Altenberger Strasse 69, 4040 Linz (Austria)

[+] These authors have contributed equally to this work.

Supporting information and the ORCID identification number(s) for the author(s) of this article can be found under: https://doi.org/10.1002/chem.201705921.

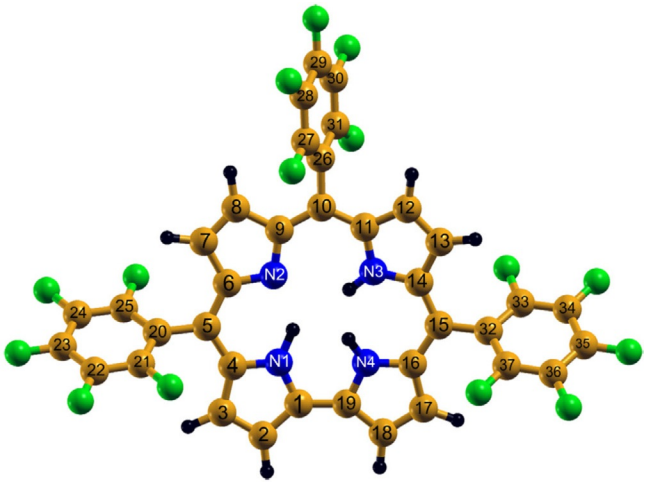

Figure 1. Schematic representation of 5,10,15-tris (pentafluorophenyl)corrole (3H-TpFPC). C, N, F, and H atoms are represented in brown, blue, green, and black, respectively. The macrocycle consists of one iminic (=N) and three aminic (–NH) nitrogen atoms (labeled as N2, and N1, N3, N4, respectively). The C atoms within the macrocycle are labeled from 1 to 19. Those within the phenyl rings are labeled from 20 to 37. The pyrrole rings are connected to each other via *meso* carbon atoms 5, 10, and 15 and a direct C1–C19 bond. The three fluorophenyl rings (C_6F_5) are substituted at the three *meso* positions 5, 10, and 15.

the detailed microstructure of the investigated system. Specific resonances can often be assigned to known building blocks and thus enable chemical changes to be tracked. Furthermore, the intensity dependence of the resonance peaks on the orientation of the surface with respect to the polarization of the radiation (hence the incident angle) enables conclusions on the direction of interatomic bonds with respect to the substrate. These means of characterization have helped in the understanding of reactions, such as cyclodehydrogenation,[30,31] amino acid decomposition,[32] and various coupling processes[33–36] even without extensive theory support. However, the assignment of the peaks to the corresponding moiety is often challenging in the case of systems with multiple subunits that provide a large number of resonances at overlapping energies.[37,38] In such cases, predictive-quality calculations are not only extremely helpful, but are even required for the interpretation of the experimental data. In this context, different approaches,[39–49] based on, for example, band-structure calculations,[40] constrained DFT calculations,[41] and cluster models,[42–45] have been applied for various surface-related molecular structures yielding reasonable agreement with experiment. Calculations of NEXAFS cross-sections employing plane-wave-based DFT calculations have recently been reported by Fratesi et al. for rather symmetric, structurally planar molecules.[48,49]

Herein, we have analyzed the on-surface chemistry of a complex 2D molecular system featuring multiple potential reaction sites and demonstrated that by combining angle-resolved NEXAFS information with high-level theoretical modeling the system's chemical conversions can be understood at the microscopic level. After fabricating a condensed, ultra-pure thin corrole film ((sub)monolayer regime) on the Ag(111) surface in UHV at 200 K, we have taken reference X-ray absorption spectroscopy (XAS) spectra for the as-deposited low-temperature phase and their subsequent changes corresponding to the geometries of the singly dehydrogenated molecules (annealed to 330 K, 2H-TpFPC·) and apparently ring-closed species (annealed to 430 K, 2H-TpFPC·(rc)). The experimental spectra and their changes corresponding to different corrole species are convincingly interpreted by means of DFT calculations. Thereby, NEXAFS spectroscopy is shown to be capable of discriminating even between highly similar structures such as tautomeric or isomeric configurations. As such, it represents a powerful tool to identify unknown compounds and to explore on-surface reactions.

Results and Discussion

Analysis of the as-grown low-temperature phase

We start our theoretical investigation by determining the most favorable adsorption geometry of single 3H-TpFPC molecules on the Ag(111) surface. We probed a number of plausible starting configurations. In its most stable configuration, a 3H-TpFPC molecule adsorbs with its macrocycle almost parallel to the underlying substrate. It is tilted by about 20° (α) with respect to the surface (Figure 2, see also the Supporting Information Figure S1).

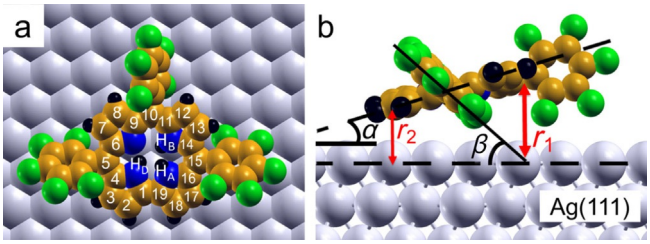

Figure 2. a) Top-view and b) side view of a single 3H-TpFPC molecule adsorbed on Ag(111) in the most stable structure. With respect to macrocyclic plane, the inner hydrogen atom H_A is shifted upwards, H_B downwards (or oppositely), whereas H_D is almost in plane. The macrocyclic C atoms are numerated from 1 to 19. The quantity r_1 (r_2) is the vertical distance between the *meso* C10 (C1/ C19) and the underlying surface. The tilt angles of the macrocycle α and of the phenyl rings β with respect to the surface are also indicated.

Thereby, the C1–C19 bond is closer to the surface, whereas the central pentafluorophenyl ring (in *meso* position 10) is pushed upward and rotated by about 66° with respect to the surface. The other two fluorophenyl rings in *meso* positions 5 and 15 (Figure 1) are rotated in a similar fashion. Both exhibit a rotation angle β of about 37°. It is important to note, that the 3H-TpFPC molecules interact rather weakly with the Ag(111) substrate. An analysis of calculated charge densities yields only minor charge transfer (below 0.2 electrons) and excludes covalent bonding between the molecule and substrate. The molecules adsorb at relatively large distances ($r_1 = 4.6$ Å, $r_2 = 3.6$ Å, Figure 2) as dictated by the dominating weak van der Waals interactions. Notably, given that the correct molecular adsorption

geometries are used, the calculated XAS spectra for both K-edges (N as well as C) are not considerably modified by the presence of the substrate (see also Figure S2, Supporting Information); the related shifts are mainly due to that of the underlying core-level shift (CLS)[39] and are calculated to be below 0.1 eV. Therefore, if not stated otherwise, the calculated spectra are obtained for structures relaxed on the surface but without considering the surface explicitly in the XAS calculations. This reduces the numerical costs for the XAS spectra by about two orders of magnitude and allows for a systematic comparison of a large number of different structures.

As a starting point for the experimental characterization of surface-supported thin films, we deposited a submonolayer coverage (nominally 0.9 ML, see Methods) of 3H-TpFPC onto the Ag(111) surface held at 200 K. We performed angle-dependent C K-edge NEXAFS measurements to characterize the spectral signature and the conformational properties of the film. Figure 3a presents three spectra taken at different incident angles θ. Within the π^* region (283–290 eV), four maxima are distinguishable (A, B, C, and D at binding energies of 284.5, 285.8, 287.9, and 289.1 eV, respectively). Broad resonances are superimposed onto the ionization edge in the σ^* region (above 290 eV). A pronounced dichroism in the spectra indicates the existence of a predominant conformation of the corrole adsorbed in a well-ordered fashion. The spectra exhibit a strong similarity to the multilayer data[27] in terms of the overall appearance and energetic positioning of the characteristic features (A–D in the π^* region), with only a slight broadening presumably induced by the minor influence of the noble metal support on the unoccupied orbitals.

As described, in Ref. [38] and in Methods, a direct curve-fitting analysis of the experimental angle-dependent NEXAFS measurements at the carbon K-edge is able to provide an estimate of the average adsorption geometry, at least a rough estimate. Exhibiting different angular dependence, the spectra close to the edge can be decomposed into two types of contributions (see Figure 3c as a zoom into the π^* region of the 25° spectrum). Those showing strong angular dependence (blue) are attributed to the macrocycle carbon atoms; the others are attributed to the pentafluorophenyl rings. The trends of the normalized intensities (symbols) are then provided as a function of the incident angle θ displayed in Figure 3d, in which they are compared to theoretical curves predicted for a π system on a threefold symmetric surface (red curves).[38] Based on this analysis, we estimate the following adsorption geometry: the macrocycle is tilted by approximately $30\pm5^\circ$ (α) and the fluorophenyl rings are rotated by $\beta=50\pm5^\circ$ (see also Figure S3, Supporting Information) with respect to the surface. In particular, the latter value (β) is in notably well agreement with the DFT-calculated structure: by weighting the three derived values (37, 37, and 66°) with the respective angle (θ)-integrated analytical cross-section expected from a Stöhr-analysis[38] (see also Methods), we obtain an effective average of about 48°.

The angle-dependent C K-edge NEXAFS spectra of the isolated adsorbed molecule (Figure 2) are calculated in order to interpret the experimental data. In Figure 3b we show the results for the incident angles of 25, 53, and 90°. We briefly note that for the 3H-TpFPC monolayer (see Figure S4, Supporting Information) almost the same spectra are calculated. The calculations exhibit excellent agreement with the experimental spectra in terms of positions of the characteristic maxima. Within the π^* region, the first three peaks A′, B′, and C′ are at binding energies of 284.5, 285.8, and 287.8 eV, respectively. Also, the B/A intensity ratio of the first peaks agrees with that in the experimental spectra even following the same trend while increasing with angle θ. Furthermore, the calculated intensities of the individual peaks correlate qualitatively with the meas-

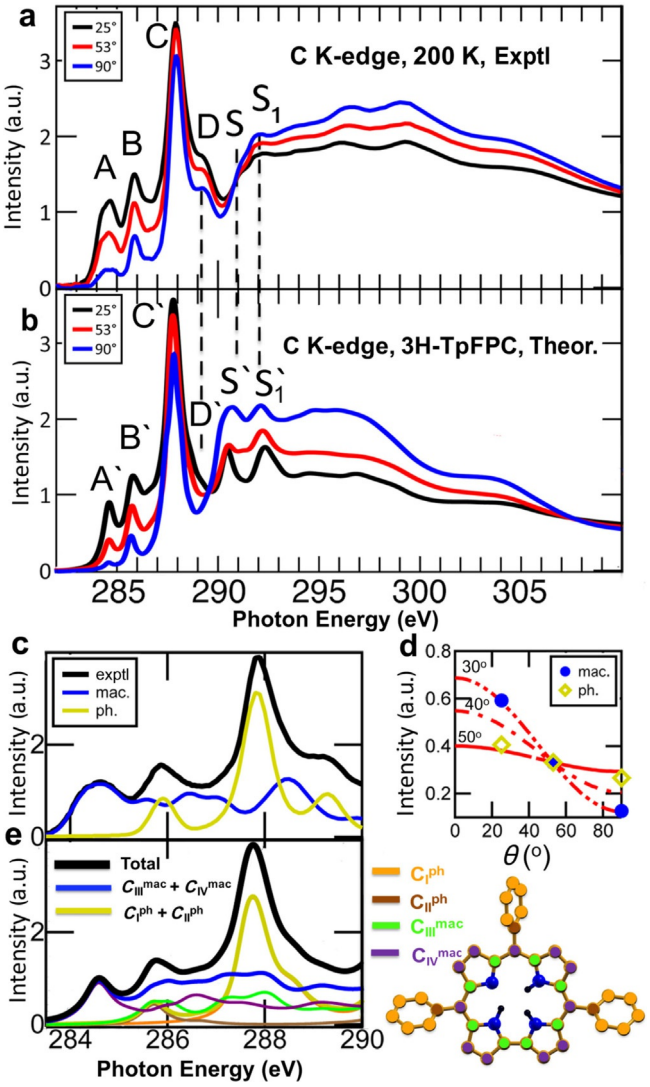

Figure 3. a) Measured angle-dependent C K-edge NEXAFS spectra of 3H-TpFPC deposited onto the Ag(111) substrate at 200 K for 25, 53, and 90° incidence. b) Calculated NEXAFS C K-edge spectra for DFT-optimized 3H-TpFPC geometries (incident angles as reported in the experiment), whereby experimental CLS have been used to align the contributions of individual atoms. c) Zoom into the π^* region of the 25° experimental spectrum deconvoluted into macrocyclic (blue) and fluorophenylic (yellow) contributions. d) Tilt angles of the macrocycle ($\approx$30°) and the fluorophenyl groups (50°) derived from (c) and related angle-dependent data. e) Zoom into the π^* region of the theoretical 25° spectrum; besides the different C types (see right panel), also the macrocyclic (blue) and the fluorophenylic (yellow) contributions are shown.

urements, where they decrease for larger incident angles within the π* region and behave oppositely within the σ* regions. We show a zoom into the π* region of the 25° spectrum to comprehensively decompose the total spectrum into the corresponding contributions of the four carbon types (Figure 3e). Similar to the multilayer system,[27] the peak A′ results only from excitations of C_{IV}^{mac} carbon atoms into the lowest macrocyclic π* orbitals. The peak B′ includes contributions from both macrocyclic (C_{III}^{mac}, C_{IV}^{mac}) and fluorophenylic (C_{II}^{ph}) atoms. Peak C′ includes contributions from the macrocyclic C_{III}^{mac} and C_{IV}^{mac} atoms, but it is dominated by excitations of the fluorophenylic C_{I}^{ph} atoms into the lowest macrocyclic π* orbitals. Obviously, the macrocyclic contributions (A′ and partially B′) have been largely suppressed for $\theta = 90^{\circ}$ as a result of the nearly planar geometry of the corrole macrocycle. Note that despite the generally good agreement, similar to the multilayer system, there are some discrepancies for energies above the main peak C: 1) The peak D is less discernible in the calculated spectra and 2) the S peak is predicted to be shifted to lower binding energies in contrast to a shift to higher energies for multilayer structures. Importantly, the calculated anisotropy in the S/S1 range is predicted to be much stronger than in the measurement at which it almost vanishes.

This discrepancy might be partially traced back to the employed semilocal exchange-correlation functionals and the approximate description of excitonic effects (see also Methods). Furthermore, we have to note here that a 1:1 theoretical modeling of this special experimental situation is impossible. For the as-deposited (200 K) sample, the experimental situation clearly deviates from an ideal periodic model. The NEXAFS measurements perform a macroscopic average and, thus, they might include signals from molecules with differently oriented fluorophenyl side groups due to 1) molecules in different islands, 2) molecules being adsorbed at step edges and surface defects, and 3) molecules in disordered and partially overlapping configurations. Nevertheless, the experimental results exhibit in many respects the same tendency as the calculated model structure of isolated molecular adsorbates.

We also measured angle-dependent XAS N K-edge spectra (Figure 4a) on the same sample as used for Figure 3, that is, with a coverage of 0.9 ML. The sample was kept at 200 K during the whole measurement procedure. The N K-edge data (Figure 4a) show a clear dichroism confirming the preferentially ordered molecular arrangement indicated by the C K-edges. The measured and calculated spectra show a vanishing dichroism at 404.0 and 403.8 eV, respectively (the resulting crossing points in Figure 4a and b separate the π* and σ* spectral regions). Within the π* region four peaks can be identified for each spectrum (E, F, G, and H at 398.4, 400.4, 402.0, and 403.2 eV), while a further peak I (407.0 eV) is found within the σ* region. The calculated N K-edge spectra agree with the experimental data very well, regarding the energetic positions of the peaks (E′, F′, G′, and H′ at 398.4, 400.6, 401.8, and 402.9 eV) as well as the angle-dependence of the peak intensities (Figure 4b). Only, the relative intensities of the peaks differ somewhat from the experiment, most noticeable for peak E which is more prominent in the experiment. An analysis of the contributions of the individual nitrogen atoms to the total edge (Figure 4c) reveals that the peak (E′) results from the N 1s transitions of the iminic N2 atom into the unoccupied π* molecular orbitals (red line), whereas the other peaks contain contributions from all N atoms into the higher laying orbitals. Thus, the intensity of this first resonance is sensitive to the amount of iminic nitrogen species in the sample and should increase when 3H-TpFPC is converted to 2H-TpFPC•. Indeed, when comparing the XPS N1s signature of this film to a multilayer (see Figure S5a,b, Supporting Information) it indicates that approximately every forth molecule of the experimental film has undergone the dehydrogenation reaction discussed in the next section. This demonstrates that the predictive power of our calculations is high enough to enable the identification of imperfections in realistic samples. Noteworthy, quantitatively de-

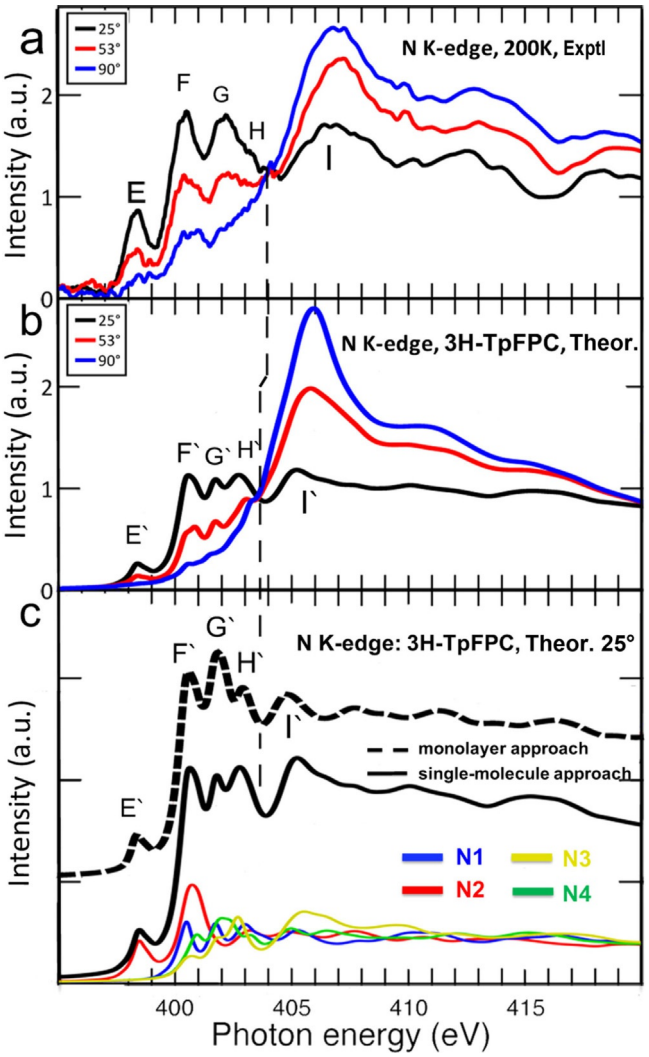

Figure 4. a) Experimental NEXAFS spectra of the N K-edge as deposited onto the substrate and measured at 200 K for 25, 53, and 90° incidences. b) Calculated angle-dependent N K-edge NEXAFS spectra of the structure shown in Figure 2 for the respective incident angles. c) Zoom into the π* region of the 25° DFT-calculated spectra for single molecule as well as monolayer adsorption. Thereby, the contributions of the different N atoms (Figure 1) are shown. The vertical hairline highlights the crossing point separating the π* and σ* regions.

termining the ratio of chemical species from XPS intensities alone is prone to artefacts from diffraction effects,[43] thus our independent NEXAFS-based analysis helps to improve the validity of the chemical analysis. When inspecting the higher energy resonance, mainly G′ and H′, the relative intensity of G is more dominating in the experiment. A similar dominating resonance G′ is present in the theoretical spectrum of a periodic monolayer (see Figure S4, Supporting Information). This again demonstrates how sensitive features of NEXAFS signatures are to the local environment.

Characterization of 2H-TpFPC· on Ag(111)

We reported earlier,[29] that annealing temperatures in the range of 300 to 360 K trigger a dehydrogenation process whereby one of the three pyrrolic nitrogen atoms (N–H; Figure 1, N1, N3, N4) gets converted to an iminic (N=) species (the resulting product was denoted as 2H-TpFPC·). When the reaction takes place for all molecules of a sample, a change of the related N–H/N= XPS peak intensity ratio from 3:1 to 2:2 is expected. Thereby, the site of the chemical conversion remains elusive to XPS as illustrated by our calculations (Figure S6, Supporting Information). We will now analyze 2H-TpFPC· films and demonstrate that NEXAFS is sensitive to the dehydrogenation place.

The structure of an ideal, periodic monolayer of 2H-TpFPC· on Ag(111) as obtained by geometry-relaxation is depicted in Figure 5a. Note, that this arrangement is in agreement with STM patterns obtained after annealing to 360 K.[28] The required lateral reorganization from the 200 K phase to this structure is facilitated by a large mobility of the individual, weakly van der Waals-bound molecular species with calculated migration barriers below 25 meV (Figure S1, Supporting Information). Figures 5b,c show that the geometric changes in the individual molecular species within the periodic layer are indeed restricted to a planarization of the remaining N–H bonds within the macrocycle of the 2H-TpFPC· molecule. According to our DFT calculations, the dehydrogenation step leaves the adsorption geometry of the individual molecules almost unchanged: the macrocycle exhibits again a tilting angle of almost 20°; the pentaflurophenyl rings are, respectively, inclined in the *meso* positions 5/15 and 10 by 37 and 65° (weighted average of ≈48°, see Methods and Ref. [38]) with respect to the surface plane.

For further comparison with theory, we prepared a submonolayer sample with a coverage of 0.4 ML by evaporating molecules onto the Ag(111) surface held at room temperature. The XPS N1s signature of this film (see Figure S5c, Supporting information) suggests that dehydrogenation occurred for ≈90% of the molecules, thus the film is closely related to the theoretical model. Again, NEXAFS C K-edge absorption spectra were recorded. Figure 5d compares exemplarily the measured $\theta = 25°$ curve of this sample with that of the previous one (cf. Figure 3; the data for 53 and 90° are shown in Figure S7, Supporting Information). Overall, the spectra of the two phases are similar, but a characteristic feature distinguishes them. A new shoulder Cp is present at 287 eV in the spectrum of the

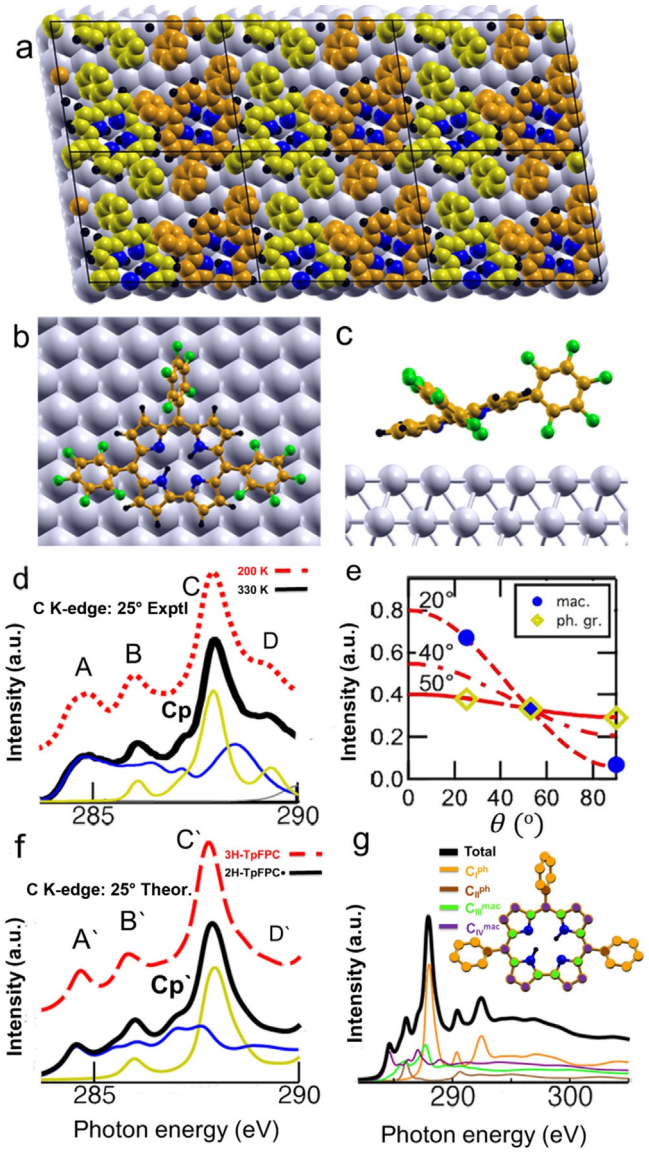

Figure 5. a) Top view of a monolayer 2H·TpFPC· on Ag(111) reported in Refs. [28] and [29]. Each unit cell contains two differently oriented (and colored) molecules. b) Top and c) side views of a single 2H-TpFPC· molecule on Ag(111) relaxed by DFT calculations. d) Measured and f) calculated NEXAFS C K-edge of 2H-TpFPC· compared to that of 3H-TpFPC for $\theta = 25°$, with a decomposition into macrocyclic (blue) and fluorophenylic (yellow) parts. e) Tilt angles of the macrocycle (≈20°) and the fluorophenyl groups (50°) derived from the angle-dependence of the different contributions depicted in (d, bottom). g) Decomposition of the total C K-edge spectra of 2H-TpFPC· into contributions of different C types (shown for $\theta = 25°$).

dehydrogenated 2H-TpFPC· samples. As shown in Figure 5f it is also predicted within the theoretical C K-edge spectrum (Cp′) and originates from the macrocyclic C_{III}^{mac} and C_{IV}^{mac} carbon atoms (all except those in the *meso* positions 5, 10, and 15; Figure 5g). The Cp′ feature, thus, can serve as an indicator for the existence of dehydrogenated 2H-TpFPC· species, whereby its intensity can be related to the number of radicals within the sample.

Again, we curve-fitted the C K-edge by assuming a π system on a threefold symmetric surface as already described in the previous section (Figure 5e). The resulting curves indicate a

tilting angle $\beta = 50 \pm 5^\circ$ for the fluorophenyl rings and a considerably flattened orientation of the macrocycle $\alpha = 20 \pm 5^\circ$, which is now in complete agreement with the calculated adsorption geometries.

For investigation of the influence of the dehydrogenation on the N K-edge we prepared a sample with a coverage of 0.8 ML by evaporating molecules on the silver surface held at 200 K and subsequent annealing to 330 K for 10 min. Utilizing the same sample as for the C K-edges was hampered by the insufficient signal-to-noise ratio due to its lower coverage. The spectra representing the annealed phase (330 K; black curve) are compared to those of the low temperature phase (200 K; red curve) in Figure 6a, in which only the $\theta = 25^\circ$ curves are

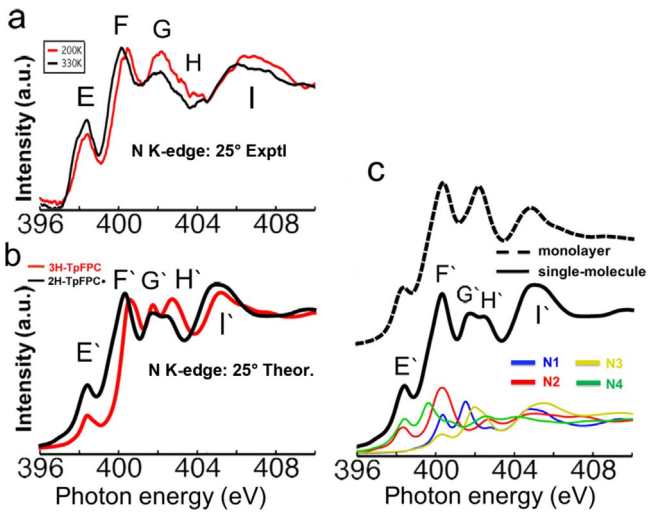

Figure 6. a) Measured and b) calculated NEXAFS N K-edge of the phase annealed at 330 K (2H-TpFPC•) compared to that of as deposited 200 K (3H-TpFPC); c) Decomposition of the total N K-edge spectra of 2H-TpFPC• into contributions of different N types. The total spectrum corresponding to single molecule adsorption (full line) is in good agreement with that of monolayer coverage (dashed line). All spectra belong to $\theta = 25^\circ$ incidence.

displayed as they exhibit the clearest features. Obviously, the intensities of peaks E and G (together with the shoulder H) are increased. The peaks F to I are rigidly shifted in energy by $\approx$0.3 eV towards lower photon energies.

In Figure 6b the theoretical N K-edges XAS spectra of 3H-TpFPC (red) and 2H-TpFPC• (black) calculated for the single molecule are compared. The simulations reproduce the experimentally observed redshift (Figure 6a) with almost 0.4(1) eV for the peaks F′–I′. The increase of the intensity of peak E′ is more pronounced in the theoretical spectra. The decomposition of the 2H-TpFPC• spectrum into contributions of the individual nitrogen atoms (Figure 6c, in which contributions from aminic-NH atoms N3, N1, and iminic =N atoms N2 and N4 are depicted) illustrates that the peak E′ originates now predominantly from N 1s transitions of both iminic atoms, N4 and N2, into the unoccupied π^* molecular orbitals. Thus, the dehydrogenation of the N4 atoms results in an initial state shift of the related resonance. Inspection of the XPS N1s signature of this film (see Figure S5d, Supporting Information) indicates that almost three out of four molecules are actually dehydrogenated. Thus, the smaller increase of the intensity of peak E in experiment represents the smaller percentage of molecules changing their chemical state as compared to the ideal theoretical cases. The other peaks contain contributions from all N atoms into the higher lying π^* orbitals, each shifted correspondingly to the lower binding energies, because they all carry contributions related to N4. Despite the energy shift, the spectral shape of each N atom remains almost the same. Obviously, hydrogen release from the N4 atom also affects all other N. This is in line with the observation of a Kondo signature related to unpaired electrons statistically distributed over the entire macrocycle.[29]

To further demonstrate the chemical sensitivity of our approach, we also calculated the N K-edge of the periodic structure (Figure 5a) of 2H-TpFPC• and depicted it on Figure 6c, top). The corresponding spectrum is in good agreement with that of the single molecule counterpart. However, there is a moderate change in the features G′ and H′, where they appear as a single peak and resemble the experimental spectrum more closely. This demonstrates that even minor intermolecular interactions have impact on the NEXAFS spectra and that our approach captures their essential influence.

To test the ability of our approach to recognize distinct contributions of different species, we analyzed the influence of the dehydrogenation site on the N K-edge spectra, that is, for all tautomeric structures of 2H-TpFPC• (Figure 7). We denote the

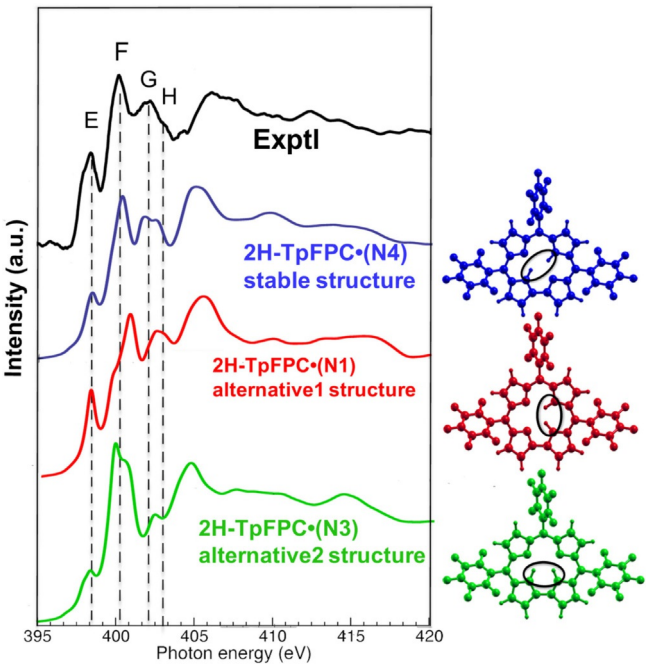

Figure 7. Comparison of the measured and calculated NEXAFS N K-edge of the most stable structure 2H-TpFPC• (N4) and the two tautomeric alternatives 2H-TpFPC• (N1/N3). All spectra are shown for $\theta = 25^\circ$. The most stable structure (blue) results from cleavage of the N4–H bond, whereas the alternatives 1/2 (red/green) are a consequence of hydrogen release from the N1–H and N3–H bond, respectively. The corresponding structures are depicted in the right panel. Vertical lines denote the energetic positions (photon energies) of the peaks in the experimental spectrum.

species according to the position of the released H atom. Both tautomeric alternatives, 2H-TpFPC• (N1) (red) and 2H-TpFPC• (N3) (blue), exhibit a more pronounced buckling of the macrocycle due to shorter H to H distances (see black ovals in Figure 7) than the already discussed structure 2H-TpFPC• (N4). In both alternatives, significant differences between the DFT-calculated N K-edge spectra and the measurement are observed: The peak F at 400.2 eV splits up into a double peak, whereas the pairs G and H (at 402.0 and 403.0 eV) appear as a small peak at 402.6 eV. According to our calculations, the tautomeric structures 2H-TpFPC• (N1/N3) can be excluded from contributing dominantly to the observed spectra, thus our approach has the capability of resolving products resulting from site-selective reactions. This is notable, since XPS spectroscopy cannot clearly distinguish between these tautomeric structures (see also Figure S6, Supporting Information).

Characterization of 2H-TpFPC·(rc) on Ag(111)

As indicated by the C 1s XPS spectra,[29] further annealing to 430 K induces C-related chemical reactions, most probably a ring-closure reaction between one of the phenyl rings and the central pyrrole moiety.[29] However, XPS spectroscopy is not sensitive to the site-selectivity of this ring-closure reaction towards 2H-TpFPC•(rc) (see also Figure S8, Supporting Information). Due to the asymmetry of the molecules (the inequivalence of the phenyl rings) the site of the chemical reaction is expected to be decisive for the properties of the resulting molecular species and possible follow-up product. This molecular transformation is indeed accompanied by a characteristic change of the molecular layer into a hexagonal arrangement (Figure 8a).[29] Figures 8b,c show top and side views of one of (in total six) possible singly ring-closed molecules arranged in hexagonal configurations on the surface. While the phenyl rings in the *meso* positions 5 and 10 are still inclined by about 37 and 67°, respectively, the phenyl ring in the *meso* position 15 is now almost parallel to the surface. This ring-closed corrolic species, thus, exhibits a flattened adsorption geometry compared to the two previously discussed cases; notably, the macrocycle shows a reduced tilt angle of $\alpha = 14^\circ$ (compared to 20° before). Note that the molecular structure can no longer be decomposed into a macrocycle and three side-groups; as a consequence, the direct curve-fitting analysis is not applicable anymore. Hence, for further analysis, we rely here completely on the theoretical spectra.

To investigate the influence of the ring closure reaction on the experimental C K-edge spectra, we annealed the 0.8 ML sample discussed in Figure 6 at 430 K for 10 min and measured its spectra. In Figure 8d, the $\theta = 25^\circ$ curve is compared to that of the previous 2H-TpFPC• dominated phase (i.e. annealed to 330 K). Despite clearly different C 1s XPS signals,[29] the C K-edges NEXAFS spectra of the two species are almost identical. However, the characteristic peak Cp has disappeared in the latter. Besides, this spectrum exhibits a new feature (highlighted by the canted arrow) at 285.2 eV, in which the valley between peaks A and B is occupied by an additional peak.

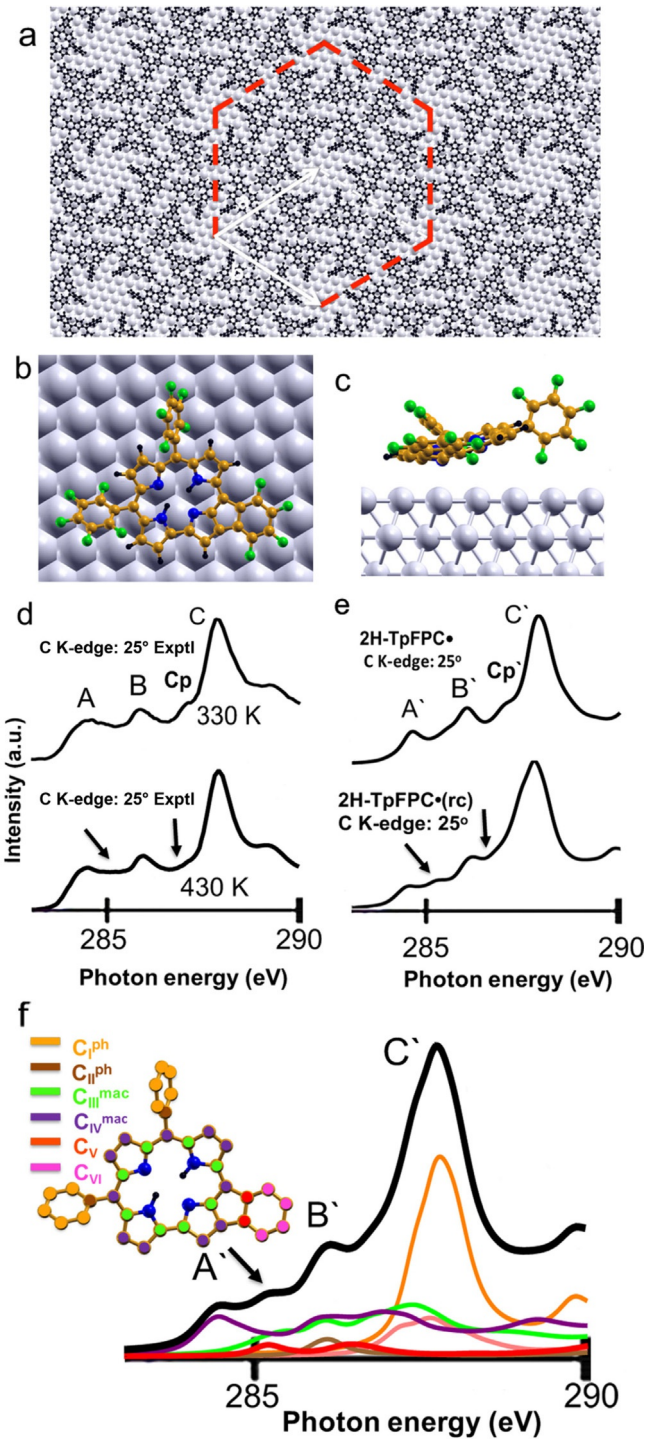

Figure 8. a) Top view of singly ring-closed corrole in a hexagonal monolayer phase (taken from Ref. [29]). $\vec{a}$, $\vec{b}$ define the unit cell of the molecular adstructure. b) Corresponding top and c) side views gained from first principles calculations. d) Measured and e) calculated C K-edge NEXAFS of 2H-TpFPC• (top) and 2H-TpFPC•(rc) (bottom), shown for an incident angle of 25°. f) Decomposition of (e, bottom) into the contribution of six C types. Canted arrows emphasize the new ring-closure-induced features. Vertical arrows mark the valley between peak B and C as an evidence of the selectivity of this reaction.

In order to identify the origin of this new peak, we calculate the corresponding C K-edges (Figure 8e). In spite of the rather

small differences between the two spectra, the new features in the 2H-TpFPC·(rc) are discernible; a canted arrow also marks the new feature at 285.2 eV. The decomposition of the DFT-calculated spectra in Figure 8 f comprises six components corresponding to the different types of carbon atoms: Besides the previously identified four C types (Figures 3 e,g), two additional components are now present, one corresponding to the two carbon atoms directly involved in the ring closure reaction and thus connecting the macrocycle with one of the phenyl rings involved in the ring-closure reaction (C_V, marked in red), and the other including the remaining C atoms in the ring-closed phenyl ring (C_{VI}, marked in pink). The latter contribute to the main peak at 288 eV and cannot be resolved experimentally. The DFT calculations interpret the new feature (at 285.2 eV) as a result of excitations of C_V atoms into the higher lying π^* states. A second peak at 287 eV originates from the same atom types; the energetic position of these two extra peaks remains almost the same regardless of the specific position of the ring closure.

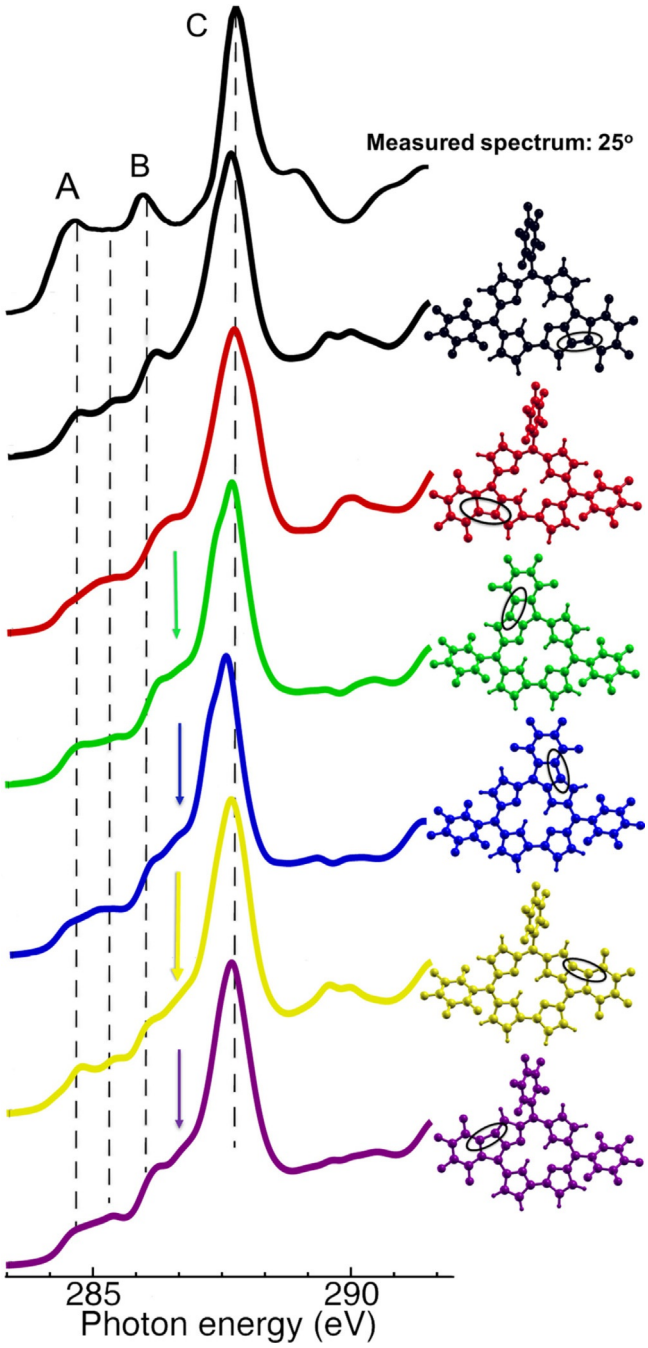

Figure 9. Experimental and calculated NEXAFS C K-edge spectra for the six possible singly ring-closed structures differing in the position of the ring closure. The black ovals highlight the carbon–carbon bond resulting from the ring-closure reaction. The colored arrows on the calculated spectra mark the most prominent deviation from the experiment.

Again, to test the ability of our approach to address the reaction-site-selectivity, we calculate the NEXAFS C K-edge spectra for the six configurations associated to the possible ring-closure reactions (Figure 9). Clearly, the valley between peak B and main peak C (marked by a vertical arrow as a guide to the eye) is site-specific: For all but the one described above configurations (C17–C37, see Figures 8 b and 9), this valley has been lifted and peak B evolves into a shoulder of the main peak C. This observation renders the C17–C37 ring-closure (black curve in Figure 9) the most likely to occur.

Conclusion

We present a comprehensive study employing the angle-resolved NEXAFS spectroscopy combined with thorough theory-guided interpretation to address on-surface site-selective chemical structure transformations. The experimental C and N K-edge NEXAFS spectra of intact 3H-TpFPC corroles and their thermally-induced derivatives adsorbed on Ag(111) are interpreted and explained in detail by means of DFT calculations of the theoretical XAS cross sections. We show that, upon annealing to 330 K, a distinctive feature in the C K-edge NEXAFS spectrum can serve as an indicator for the formation of a dehydrogenated 2H-TpFPC· species. Moreover, N K-edge NEXAFS provides detailed information on the specific N–H termination, at which hydrogen release takes place, which cannot be derived by means of N 1s XPS. A further annealing step at 430 K triggers a ring closure between one of the C_6F_5 side groups and the macrocycle. Whereas XPS is unable to unravel which of the six possible and energetically equivalent ring-closure reactions first occurs, NEXAFS spectroscopy strikingly enables us to discriminate between the different ring-closure reactions.

Our analysis convincingly demonstrates that angle-resolved NEXAFS spectroscopy combined with theory-guided interpretations based on accurate simulations provides a powerful tool for the identification and understanding of on-surface site-selective chemical structure transformations. This represents an extension of the traditional use of NEXAFS measurements for obtaining moiety-specific adsorption geometries, which is applicable to the timely topic of on-surface synthesis. The capability to resolve closely related low-symmetry structures such as tautomers and isomers is specifically attractive for the investigation of larger molecular systems featuring the same moiety at multiple sites such as tetrapyrrolic systems or conjugated hydrocarbons and related derivatives.

Methods

Sample preparation

5,10,15-Tris(pentafluorophenyl) corrole (3H-TpFPC) was synthesized according to reported procedures.[50] It was purified utilizing preparative high-performance liquid chromatography (HPLC) and subsequently analyzed by ^{1}H, ^{13}C, and ^{19}F NMR spectroscopy. Deposition and characterization of ultra-thin films on Ag(111) were carried out in experimental chambers with pressures in the low 10^{-9} mbar range or lower. The Ag(111) single-crystal surface (Surface Preparation Laboratory, polished to $<0.5^{\circ}$) was cleaned by several cycles of sputtering (Ar+, 1 kV) and annealing (720 K). 3H-TpFPC molecules were deposited by organic molecular beam epitaxy from a quartz crucible held at 500 K after prolonged degassing of the molecular powders in vacuo at 480 K for several hours. During the initial deposition of the 3H-TpFPC molecules, the Ag(111) substrate was held at 200 K. Deposition at RT already results in a disordered pattern built up by different corrolic states (see also Figure S9, Supporting Information). (Sub)monolayer growth of ultra-thin films and their subsequent thermal treatment to 330 and 430 K was characterized by combined STM and XPS. Typically, the annealed samples show well-ordered nontrivial (330 K) and hexagonal (430 K) STM structures presented in Ref. [29]. Also the as-deposited (200 K) samples can be observed in the submonolayer regime, consisting of regular islands of up to 100 nm diameter with differently oriented molecular species at an estimated coverage of approximately 0.5 monolayers, see Figure S4 in the Supporting Information.

X-ray spectroscopy

Measurements were performed at the HE-SGM dipole magnet beamline of the BESSY II synchrotron in Berlin. NEXAFS spectra were recorded at 200 K for the low temperature phase, and at RT for the subsequent derivatives, in normal emission geometry. A monochromator grating of 1500 L mm^{-1} and slit widths of 200 μm were used in partial electron yield mode at a retarding voltage of −150 and −250 V for the C and N K-edge, respectively. The spectra were measured at different incident angles θ (25, 53, and $90^{\circ}=$ normal incidence) inclined by the electric-field vector E of the incident light (linear polarization $P=90\,\%$) and the surface normal (see also Figure 10). After subtraction of the signal of the bare crystal from the averaged data, the resulting spectra were normalized to an edge jump of one. For obtaining an experimental NEXAFS tilt angle β, we employed the theoretical angle-dependences of the intensity I of a resonance corresponding to the case of threefold or higher substrate symmetry as described in Ref. [38]:

$$I(\beta,\theta) = PI^{\parallel} + (1-P)I^{\perp}$$

in which $I^{\parallel} = \frac{A}{3}\left[1+\frac{1}{2}(3\cos^2\theta-1)(3\cos^2\beta-1)\right]$, $I^{\perp} = \frac{1}{2}A\sin^2\beta$, and A accounts for the angle-integrated cross-section normalized to one.

When the same molecular moiety is present on the surface with several inclinations β_i, the determined experimental estimate is compared with the theoretical average of the DFT-calculated tilt angles of the individual moieties, weighted by the inverse angle-integrated cross-sections A_i with $A_i = \int_0^{90^{\circ}} I(\beta_i,\theta)d\theta$.

DFT calculations

For a realistic and as accurate as possible modeling of the investigated thin-film surface structures, the molecular species together with the metallic substrates have been calculated using periodic boundary conditions. The complete ad-system was modeled by periodically repeated supercells, containing slabs of four Ag layers separated by a vacuum of a thickness of 22 Å. The topmost two layers and all atoms of the molecules were allowed to relax freely, whereas the atoms in the two lowest layers were kept fixed at the ideal bulk positions. The structural relaxations were performed with convergence criteria of 0.03 eV Å^{-1} and 10^{-5} eV for forces and total energies, respectively. Due to the large lateral supercell sizes, between 26 Å×20 Å (one molecule per unit cell) and 19 Å×14 Å (two molecules per unit cell), it was found to be sufficient to sample the Brillouin zone with the Γ point. DFT calculations using the Vienna ab initio Simulation Package (VASP)[51] were performed for structural relaxation. Thereby, we employed the gradient-corrected PW91 functional[52] to account for the exchange and correlation interactions. The so-called DFT-D scheme,[53] based on the London dispersion formula, has been used to approximately account for the ubiquitous dispersion interactions. This scheme has been proven to accurately deliver the electronic and geometric properties of different systems at low computational costs.[54–60] The electron-ion interaction was described by pseudopotentials within the projector-augmented wave (PAW) method,[61] which allows for a moderate energy cutoff of 400 eV for the plane-wave basis.

The gauge including (GI-PAW) pseudopotential scheme has been used to determine the angle-dependent XAS of the optimized structures. Specifically, the Xspectra code[62,63] of the Quantum ES-

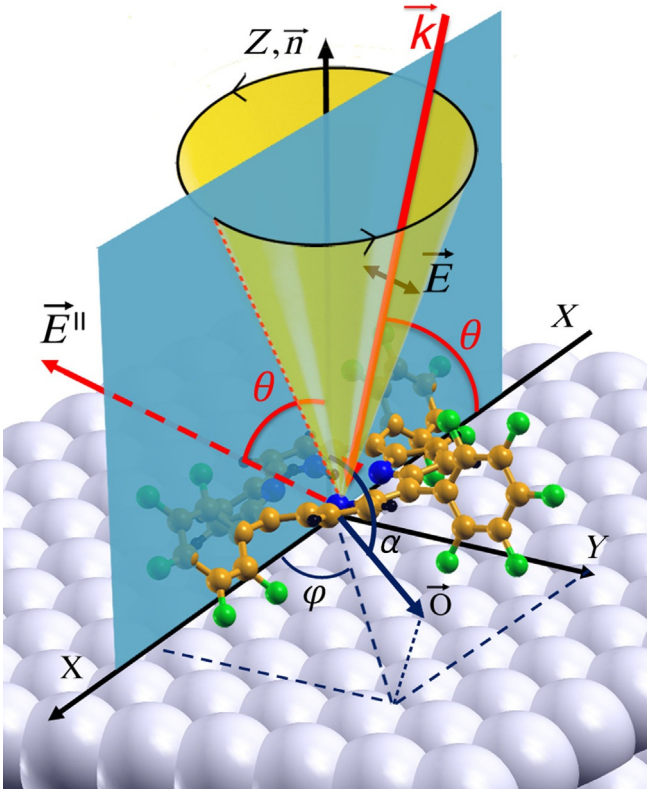

Figure 10. Sketch of the angle-dependent NEXAFS setup. The direction of a transition dipole $\vec{O}$, is defined by the angles α and φ.[38] The incident X-ray (exemplarily shown in the *xz*-plane) is tilted by θ with respect to the surface plane (tilt angle of the *E*-field component $E^{\parallel}$ with respect to the surface normal $\vec{n}$). The cross-sections σ_{XAS} are calculated without considering a "preferred molecular orientations", that is, by averaging with respect to φ (wave vector (k) at the shown cone-surface).

PRESSO (QE) package[64] was employed to calculate the NEXAFS K-edge spectra of the C and N species. Thereby the 1s core hole is incorporated by generating scalar-relativistic multiprojector GIPAW pseudopotentials with a corresponding occupation of the inner shells. This allows for a reliable, but computationally very efficient description of excitonic effects.[65] The Lanzcos recursion scheme is employed to expand the Green's function of the empty states (continued-fraction expansion).[66–68] This procedure reliably describes the near- as well as far-edge features of the absorption spectrum.[69–72] The quadrupole contributions in the pre-edge regions are found to be very small and negligible compared to those of the dipole term. Hence, we restrict the calculations to the latter. In the spectra calculations we use the same numerical parameters and physical approximation (e.g., functional) as used for the structural relaxations. The angle-dependent X-ray absorption spectra are calculated for a given wave vector k and polarization vector ε of the incident X-rays. In order to compare with the experimental situation featuring three-fold symmetry, we calculate the XAS cross-section σ_{XAS} for an electric field tilted by an angle θ with respect to the surface normal (oriented along the z-axis), averaged with respect to the azimuth angle, that is, by evaluating

$$\sigma(\theta) = {}^1\!/_2[\sigma_{XAS}(\theta,\varphi_0) + \sigma_{XAS}\ (\theta,\varphi_0 + 90^\circ)]$$

for an arbitrary angle φ_0 (Figure 10). Following the experimental measurements, we considered, in particular, the cases with $\theta = 25$, 53, and 90°.

The XAS cross-sections of each C and N atom within the relaxed structures are calculated in a 40 eV wide range above the respective K-edge. Subsequently, the total NEXAFS spectrum of the molecular system was obtained from the superposition of the individual spectra offset shifted by the corresponding CLS obtained within DFT[73–76] for each C and N atom (see Ref. [27] for further details). The overall spectra are then aligned to the respective experimental K-edges. The linewidth is chosen energy dependent[77] rising arctan-like from 0.1 eV at 395 eV (280 eV) to 1.0 eV at 435 eV (320 eV) for the N (C) K-edge spectra. By choosing the linewidth somewhat smaller than in the experimental spectra, we prevent it from masking the spectral fine structure.

Acknowledgements

This work was made possible via the Austrian Science Fund (FWF) project D-A-CH i958. Funding provided by the European Union via ERC Advanced Grant MolArt (Grant 247299), the German Research Foundation (DFG) via KL 2294/3-1, FOR 1405, and TRR 142, the Munich-Centre for Advanced Photonics (MAP), and the Austrian Science Fund (FWF-P28167) is also gratefully acknowledged. Computational resources were allocated at the Paderborn Center for Parallel Computing (PC^2). We also thank the Helmholtz-Zentrum Berlin for partial financial support and for the allocation of synchrotron radiation beam time.

Conflict of interest

The authors declare no conflict of interest.

Keywords: corroles · DFT calculations · NEXAFS · silver · XAS

[1] R. Bonnett, *Chem. Soc. Rev.* **1995**, *24*, 19–33.
[2] J. A. Shelnutt, X. Z. Song, J. G. Ma, S. L. Jia, W. Jantzen, C. J. Medforth, *Chem. Soc. Rev.* **1998**, *27*, 31–41.
[3] D. Gust, T. A. Moore, A. L. Moore, *Acc. Chem. Res.* **2001**, *34*, 40–48.
[4] S. W. Ryter, J. Alam, A. M. K. Choi, *Physiol. Rev.* **2006**, *86*, 583–650.
[5] J. M. Gottfried, H. Marbach, *Z. Phys. Chem.* **2009**, *223*, 53–74.
[6] M. Grätzel, *Acc. Chem. Res.* **2009**, *42*, 1788–1798.
[7] W. Auwärter, D. Écija, F. Klappenberger, J. V. Barth, *Nat. Chem.* **2015**, *7*, 105–120.
[8] A. W. Johnson, I. T. Kay, *J. Chem. Soc.* **1965**, 1620–1629.
[9] Z. Gross, N. Galili, I. Saltsman, *Angew. Chem. Int. Ed.* **1999**, *38*, 1427–1429; *Angew. Chem.* **1999**, *111*, 1530–1533.
[10] Z. Gross, L. Simkhovich, N. Galili, *Chem. Commun.* **1999**, 599–600.
[11] Z. Gross, G. Golubkov, L. Simkhovich, *Angew. Chem. Int. Ed.* **2000**, *39*, 4045–4047; *Angew. Chem.* **2000**, *112*, 4211–4213.
[12] L. Simkhovich, Z. Gross, *Tetrahedron Lett.* **2001**, *42*, 8089–8092.
[13] A. Mahammed, H. B. Gray, A. E. Meier-Callahan, Z. Gross, *J. Am. Chem. Soc.* **2003**, *125*, 1162–1163.
[14] Z. Gross, *J. Biol. Inorg. Chem.* **2001**, *6*, 733–738.
[15] G. Golubkov, J. Bendix, H. B. Gray, A. Mahammed, I. Goldberg, A. J. DiBilio, Z. Gross, *Angew. Chem. Int. Ed.* **2001**, *40*, 2132–2134; *Angew. Chem.* **2001**, *113*, 2190–2192.
[16] Z. Gross, H. B. Gray, *Adv. Synth. Catal.* **2004**, *346*, 165–170.
[17] S. Nardis, D. Monti, R. Paolesse, *Mini-Rev. Org. Chem.* **2005**, *2*, 355–374.
[18] I. Aviv-Harel, Z. Gross, *Chem. Commun.* **2007**, 1987–1999.
[19] L. Flamigni, D. T. Gryko, *Chem. Soc. Rev.* **2009**, *38*, 1635–1646.
[20] I. Aviv-Harel, Z. Gross, *Chem. Eur. J.* **2009**, *15*, 8382–8394.
[21] I. Aviv-Harel, Z. Gross, *Coord. Chem. Rev.* **2011**, *255*, 717–736.
[22] W. Schöfberger, F. Faschinger, S. Chattopadhyay, S. Bhakta, B. Mandal, J. A. A. W. Elemans, S. Müllegger, S. Tebi, R. Koch, F. Klappenberger, M. Paszkiewicz, J. V. Barth, E. Rauls, H. Aldahhak, W. G. Schmidt, A. Dey, *Angew. Chem. Int. Ed.* **2016**, *55*, 2350–2355; *Angew. Chem.* **2016**, *128*, 2396–2401.
[23] S. Kuck, G. Hoffmann, M. Bröring, M. Fechtel, M. Funk, R. Wiesendanger, *J. Am. Chem. Soc.* **2008**, *130*, 14072–14073.
[24] X. Miao, A. Gao, S. Hiroto, H. Shinokubo, A. Osuka, H. Xin, W. Deng, *Surf. Interface Anal.* **2009**, *41*, 225–230.
[25] S. Kuck, M. Prostak, M. Funk, M. Bröring, G. Hoffmann, R. Wiesendanger, *J. Vac. Sci. Technol. A* **2010**, *28*, 795–798.
[26] M. Rashidi, S. Müllegger, M. Roithner, W. Schöfberger, R. Koch, *J. Am. Chem. Soc.* **2012**, *134*, 91–94.
[27] H. Aldahhak, M. Paszkiewicz, F. Allegretti, D. A. Duncan, S. Tebi, P. S. Deimel, P. C. Aguilar, Y.-Q. Zhang, A. C. Papageorgiou, R. Koch, J. V. Barth, W. G. Schmidt, S. Müllegger, W. Schöfberger, F. Klappenberger, E. Rauls, U. Gerstmann, *J. Phys. Chem. C* **2017**, *121*, 2192–2200.
[28] S. Tebi, H. Aldahhak, G. Serrano, W. Schöfberger, E. Rauls, W. G. Schmidt, R. Koch, S. Müllegger, *Nanotechnology* **2016**, *27*, 025704–025708.
[29] S. Tebi, M. Paszkiewicz, H. Aldahhak, F. Allegretti, S. Gonglach, M. Haas, M. Waser, P. S. Deimel, P. C. Aguilar, Y.-Q. Zhang, A. C. Papageorgiou, D. A. Duncan, J. V. Barth, W. G. Schmidt, R. Koch, U. Gerstmann, E. Rauls, F. Klappenberger, W. Schöfberger, S. Müllegger, *ACS Nano* **2017**, *11*, 3383–3391.
[30] K. Weiss, G. Beernink, F. Dötz, A. Birkner, K. Müllen, C. H. Wöll, *Angew. Chem. Int. Ed.* **1999**, *38*, 3748–3752; *Angew. Chem.* **1999**, *111*, 3974–3978.
[31] G. Di Santo, S. Blankenburg, C. Castellarin-Cudia, M. Fanetti, P. Borghetti, L. Sangaletti, L. Floreano, A. Verdini, E. Magnano, F. Bondino, C. A. Pignedoli, M. T. Nguyen, R. Gaspari, D. Passerone, A. Goldoni, *Chem. Eur. J.* **2011**, *17*, 14354–14359.
[32] Y. Zubavichus, M. Zharnikov, A. Shaporenko, O. Fuchs, L. Weinhardt, C. Heske, E. Umbach, J. D. Denlinger, M. Grunze, *J. Phys. Chem. A* **2004**, *108*, 4557–4565.
[33] S. Weigelt, C. Busse, C. Bombis, M. M. Knudsen, K. V. Gothelf, T. Strunskus, C. Wöll, M. Dahlbom, B. Hammer, E. Lægsgaard, F. Besenbacher, T. R. Linderoth, *Angew. Chem. Int. Ed.* **2007**, *46*, 9227–9230; *Angew. Chem.* **2007**, *119*, 9387–9390.
[34] V. K. Kanuru, G. Kyriakou, S. K. Beaumont, A. C. Papageorgiou, D. J. Watson, R. M. Lambert, *J. Am. Chem. Soc.* **2010**, *132*, 8081–8086.
[35] M. Di Giovannantonio, M. El Garah, J. Lipton-Duffin, V. Meunier, L. Cardenas, Y. F. Revurat, A. Cossaro, A. Verdini, D. F. Perepichka, F. Rosei, G. Contini, *ACS Nano* **2013**, *7*, 8190–8198.

[36] A. Wiengarten, K. Seufert, W. Auwärter, D. Ecija, K. Diller, F. Allegretti, F. Bischoff, S. Fischer, D. A. Duncan, A. C. Papageorgiou, F. Klappenberger, R. G. Acres, T. H. Ngo, J. V. Barth, *J. Am. Chem. Soc.* **2014**, *136*, 9346 – 9354.
[37] G. Hähner, M. Kinzler, C. Wöll, M. Grunze, M. K. Scheller, L. S. Cederbaum, *Phys. Rev. Lett.* **1991**, *67*, 851 – 854.
[38] J. Stöhr, D. A. Outka, *Phys. Rev. B* **1987**, *36*, 7891 – 7905.
[39] K. Diller, R. J. Maurer, M. Müller, K. Reuter, *J. Chem. Phys.* **2017**, *146*, 214701 – 214706.
[40] E. Voloshina, R. Ovcharenko, A. Shulakov, Y. Dedkov, *J. Chem. Phys.* **2013**, *138*, 154706 – 154713.
[41] G. M. Su, S. N. Patel, C. D. Pemmaraju, D. Prendergast, M. L. Chabinyc, *J. Phys. Chem. C* **2017**, *121*, 9142 – 9152.
[42] K. Diller, F. Klappenberger, F. Allegretti, A. C. Papageorgiou, S. Fischer, A. Wiengarten, S. Joshi, K. Seufert, D. Écija, W. Auwärter, J. V. Barth, *J. Chem. Phys.* **2013**, *138*, 154710 – 154718.
[43] K. Diller, F. Klappenberger, M. Marschall, K. Hermann, A. Nefedov, Ch. Wöll, J. V. Barth, *J. Chem. Phys.* **2012**, *136*, 014705 – 014717.
[44] K. Diller, Y. Ma, Y. Luo, F. Allegretti, J. Liu, B. Z. Tang, N. Lin, J. V. Barth, F. Klappenberger, *Phys. Chem. Chem. Phys.* **2015**, *17*, 31117 – 31124.
[45] C. Kolczewski, K. Hermann, *Surf. Sci.* **2004**, *552*, 98 – 110.
[46] S. N. Patel, G. M. Su, C. Luo, M. Wang, L. A. Perez, D. A. Fischer, D. Prendergast, G. C. Bazan, A. J. Heeger, M. L. L. Chabinyc, E. J. Kramer, *Macromolecules* **2015**, *48*, 6606 – 6616.
[47] K. M. O'Donnell, H. Hedgeland, G. Moore, A. Suleman, M. Siegl, L. Thomsen, O. Warschkow, S. R. Schofield, *Phys. Chem. Chem. Phys.* **2016**, *18*, 27290 – 27299.
[48] G. Fratesi, V. Lanzilotto, S. Stranges, M. Alagia, G. P. Brivio, L. Floreano, *Phys. Chem. Chem. Phys.* **2014**, *16*, 14834 – 14844.
[49] G. Fratesi, V. Lanzilotto, L. Floreano, G. P. Brivio, *J. Phys. Chem. C* **2013**, *117*, 6632 – 6638.
[50] L. M. Reith, M. Stiftinger, U. Monkowius, G. Knör, W. Schöfberger, *Inorg. Chem.* **2011**, *50*, 6788 – 6797.
[51] G. Kresse, J. Furthmüller, *Comput. Mater. Sci.* **1996**, *6*, 15 – 50.
[52] J. P. Perdew, J. A. Chevary, S. H. Vosko, K. A. Jackson, M. R. Pederson, D. J. Singh, C. Fiolhais, *Phys. Rev. B* **1992**, *46*, 6671 – 6687.
[53] F. Ortmann, F. Bechstedt, W. G. Schmidt, *Phys. Rev. B* **2006**, *73*, 205101 – 205110.
[54] H. Aldahhak, W. G. Schmidt, E. Rauls, *Surf. Sci.* **2015**, *641*, 278 – 281.
[55] H. Aldahhak, S. Matencio, E. Barrena, C. Ocal, W. G. Schmidt, E. Rauls, *Phys. Chem. Chem. Phys.* **2015**, *17*, 8776 – 8783.
[56] C. Braun, S. Sanna, W. G. Schmidt, *J. Phys. Chem. C* **2015**, *119*, 9342 – 9346.
[57] Q. Wu, C. Li, L. Tan, Z. Hang, W. Zhu, *RSC Adv.* **2016**, *6*, 48489 – 48497.
[58] G. Zhang, X. Xiang, F. Yang, L. Liu, T. Tang, Y. Shi, X. Wang, *Phys. Chem. Chem. Phys.* **2016**, *18*, 15711 – 15718.
[59] A. Benghia, T. Dahame, B. Bentria, *Opt. Mater.* **2016**, *54*, 269 – 275.
[60] C. Lechner, B. Pannier, P. Baranek, N. C. Forero-Martinez, H. Vach, *J. Phys. Chem. C* **2016**, *120*, 5083 – 5100.
[61] G. Kresse, D. Joubert, *Phys. Rev. B* **1999**, *59*, 1758 – 1775.
[62] M. Taillefumier, D. Cabaret, A. M. Flank, F. Mauri, *Phys. Rev. B* **2002**, *66*, 195107 – 195114.
[63] C. Gougoussis, M. Calandra, A. P. Seitsonen, F. Mauri, *Phys. Rev. B* **2009**, *80*, 075102 – 075109.
[64] P. Giannozzi, S. Baroni, N. Bonini, M. Calandra, R. Car, C. Cavazzoni, D. Ceresoli, G. L. Chiarotti, M. Cococcioni, I. Dabo, A. Dal Corso, S. de Gironcoli, S. Fabris, G. Fratesi, R. Gebauer, U. Gerstmann, C. Gougoussis, A. Kokalj, M. Lazzeri, L. Martin-Samos, N. Marzari, F. Mauri, R. Mazzarello, S. Paolini, A. Pasquarello, L. Paulatto, C. Sbraccia, S. Scandolo, G. Sclauzero, A. P. Seitsonen, A. Smogunov, P. Umari, R. M. Wentzcovitch, *J. Phys. Condens. Matter* **2009**, *21*, 395502 – 395520.
[65] R. Buczko, G. Duscher, S. J. Pennycook, S. T. Pantelides, *Phys. Rev. Lett.* **2000**, *85*, 2168 – 2171.
[66] C. Lanczos, *J. Res. Natl. Bur. Stand.* **1952**, *49*, 33 – 53.
[67] R. Haydock, V. Heine, M. J. Kelly, *J. Phys. C* **1975**, *8*, 2591 – 2605.
[68] B. Walker, R. Gebauer, *J. Chem. Phys.* **2007**, *127*, 164106 – 164114.
[69] E. Gaudry, D. Cabaret, C. Brouder, I. Letard, A. Rogalev, F. Wilhlem, N. Jaouen, P. Sainctavit, *Phys. Rev. B* **2007**, *76*, 094110 – 094119.
[70] A. Juhin, C. Brouder, M. A. Arrio, D. Cabaret, P. Sainctavit, E. Balan, A. Bordage, A. P. Seitsonen, G. Calas, S. G. Eeckhout, P. Glatzel, *Phys. Rev. B* **2008**, *78*, 195103 – 195120.
[71] D. Cabaret, F. Mauri, G. S. Henderson, *Phys. Rev. B* **2007**, *75*, 184205 – 184213.
[72] C. Ehlert, W. E. S. Unger, P. C. Saalfrank, *Phys. Chem. Chem. Phys.* **2014**, *16*, 14083 – 14095.
[73] S. García-Gil, A. García, P. Ordejón, *Eur. Phys. J. B* **2012**, *85*, 239 – 248.
[74] O. Bunău, M. Calandra, *Phys. Rev. B* **2013**, *87*, 205105 – 205116.
[75] G. M. Rignanese, A. Pasquarello, *Surf. Sci.* **2001**, *490*, L614 – L618.
[76] G. M. Rignanese, A. Pasquarello, *Phys. Rev. B* **2001**, *63*, 075307 – 075316.
[77] O. Bunău, Y. Joly, *J. Phys. Condens. Matter* **2009**, *21*, 345501 – 345511.

Manuscript received: December 13, 2017
Revised manuscript received: February 19, 2018
Accepted manuscript online: March 1, 2018
Version of record online: April 23, 2018